Novel Knob-integrated fiber Bragg grating sensor with polyvinyl alcohol coating for simultaneous relative humidity and temperature measurement

Guofeng Yan,[1,*] Yanhong Liang,[1] El-Hang Lee,[1] and Sailing He[1,2]

[1] *Centre for Optical and Electromagnetic Research, State Key Laboratory of Modern Optical Instrumentation, Zhejiang Provincial Key Laboratory for Sensing Technologies, Zhejiang University, Hangzhou 310058, China*
[2] *Department of Electromagnetic Engineering, School of Electrical Engineering, Stockholm S-100 44, Sweden*
[*] *yanguofeng@zju.edu.cn*

Abstract: A novel high performance optical fiber sensor for simultaneous measurement of relative humidity (RH) and temperature based on our newly designed knob-integrated fiber Bragg grating (FBG) is proposed and experimentally demonstrated. The knob-shaped taper followed by an FBG works as a multifunctional joint that not only excites the cladding modes but also recouples the cladding modes reflected by the FBG back into the leading single mode fiber. Polyvinyl alcohol (PVA) film is plated on the fiber surface by dip-coating technique as a humidity-to-refractive index (RI) transducer, and affects the intensity of reflected cladding modes by way of evanescent fields. By monitoring the intensity and wavelength of the reflected cladding modes, the RH and temperature variance can be determined simultaneously. Experimental results show an RH sensitivity of up to 1.2 dB/%RH within an RH range of 30-95%, which is significantly better than previously reported values. And the temperature sensitivity of 8.2 pm/°C could be achieved in the temperature range of 25-60°C. A fast and reversible time response has also been demonstrated, enabling to pick up a humidity change as fast as 630 ms. The capability of simultaneous measurement of RH and temperature, the fast response, the reusability and the simple fabrication process make this structure a highly promising sensor for real-time practical RH monitoring applications.

OCIS codes: (060.2370) Fiber optics sensors; (060.3735) Fiber Bragg gratings; (310.6845) Thin film devices and applications.

References and links

1. Y. Sakai, M. Matsuguchi, and T. Hurukawa, "Humidity sensor using cross-linked poly (chloromethyl styrene)," Sens. Actuators B Chem. **66**(1-3), 135–138 (2000).
2. M. Shao, X. G. Qiao, H. W. Fu, N. Zhao, Q. P. Liu, and H. Gao, "An in-Fiber Mach–Zehnder interferometer based on arc-induced tapers for high sensitivity humidity sensing," IEEE Sens. J. **13**(5), 2026–2031 (2013).
3. S. Akita, H. Sasaki, K. Watanabe, and A. Seki, "A humidity sensor based on a hetero-core optical fiber," Sens. Actuators B Chem. **147**(2), 385–391 (2010).
4. W. C. Wong, C. C. Chan, L. H. Chen, T. Li, K. X. Lee, and K. C. Leong, "Polyvinyl alcohol coated photonic crystal optical fiber sensor for humidity measurement," Sens. Actuators B Chem. **174**, 563–569 (2012).
5. L. H. Chen, T. Li, C. C. Chan, R. Menon, P. Balamurali, M. Shaillender, B. Neu, X. M. Ang, P. Zu, W. C. Wong, and K. C. Leong, "Chitosan based fiber-optic Fabry–Perot humidity sensor," Sens. Actuators B Chem. **169**, 167–172 (2012).
6. R. Gao, Y. Jiang, and W. H. Ding, "Agarose gel filled temperature-insensitive photonic crystal fibers humidity sensor based on the tunable coupling ratio," Sens. Actuators B Chem. **195**, 313–319 (2014).
7. K. M. Tan, C. M. Tay, S. C. Tjin, C. C. Chan, and H. Rahardjo, "High relative humidity measurements using gelatin coated long-period grating sensors," Sens. Actuators B Chem. **110**(2), 335–341 (2005).
8. Y. Miao, K. Zhang, Y. Yuam, B. Liu, H. Zhang, Y. Liu, and J. Yao, "Agarose gel-coated LPG based on two sensing mechanisms for relative humidity measurement," Appl. Opt. **52**(1), 90–95 (2013).

#238178 Received 16 Apr 2015; revised 31 May 2015; accepted 1 Jun 2015; published 4 Jun 2015

9. S. F. H. Correia, P. Antunes, E. Pecoraro, P. P. Lima, H. Varum, L. D. Carlos, R. A. S. Ferreira, and P. S. André, "Optical fiber relative humidity sensor based on a FBG with a di-ureasil coating," Sensors (Basel) **12**(7), 8847–8860 (2012).
10. W. Zhang and D. J. Webb, "Humidity responsivity of poly(methyl methacrylate)-based optical fiber Bragg grating sensors," Opt. Lett. **39**(10), 3026–3029 (2014).
11. G. Rajan, Y. M. Noor, B. Liu, E. Ambikairaja, D. J. Webb, and G. D. Peng, "A fast response intrinsic humidity sensor based on an etched singlemode polymer fiber Bragg grating," Sens. Actuators A Phys. **203**, 107–111 (2013).
12. Y. P. Miao, B. Liu, H. Zhang, Y. Li, H. B. Zhou, H. Sun, W. H. Zhang, and Q. D. Zhao, "Relative humidity sensor based on tilted fiber Bragg grating with Polyvinyl alcohol coating," IEEE Photon. Technol. Lett. **21**(7), 441–443 (2009).
13. X. Dong, T. Li, Y. Liu, Y. Li, C. L. Zhao, and C. C. Chan, "Polyvinyl alcohol-coated hybrid fiber grating for relative humidity sensing," J. Biomed. Opt. **16**(7), 077001 (2011).
14. B. Gu, M. Yin, A. P. Zhang, J. Qian, and S. He, "Optical fiber relative humidity sensor based on FBG incorporated thin-core fiber modal interferometer," Opt. Express **19**(5), 4140–4146 (2011).
15. S. Q. Zhang, X. Y. Dong, T. Li, C. C. Chan, and P. P. Shum, "Simultaneous measurement of relative humidity and temperature with PCF-MZI cascaded by fiber Bragg grating," Opt. Commun. **303**, 42–45 (2013).
16. M. Yang, W. Xie, Y. Dai, D. Lee, J. Dai, Y. Zhang, and Z. Zhuang, "Dielectric multilayer-based fiber optic sensor enabling simultaneous measurement of humidity and temperature," Opt. Express **22**(10), 11892–11899 (2014).

1. Introduction

Relative humidity (RH), defined as the ratio of the partial pressure of water vapor to the saturated vapor pressure of water at a given temperature, is of great importance in various areas, including chemical process controlling, weather forecasting, agriculture, food and medical facilities [1]. Conventional RH sensors, such as mechanical hygrometers, wet and dry bulb psychrometers, electronic humidity sensors, always suffer from long response time, low sensitivity, electromagnetic inference and electric leakage by dewfall, which limit their practical applications. On the other hand, according to the definition, the relative humidity is generally associated with temperature, and so it is necessary for simultaneous measurement of humidity and temperature. However, the conventional RH sensors can only monitor the RH information and it usually needs other sensors to realize real time temperature monitoring. Thus new type of sensors enabling simultaneous RH and temperature measurement are in huge demands.

Due to their small sizes, fast response, high sensitivity, remote operation capability and potential for distributed sensing, fiber-optic RH sensors have been widely developed in the past few decades based on different configurations with sensing film coatings [2–16]. The modal interferometer is one kind of the commonly used structures for RH sensing, such as Mach-Zehnder interferometer based on two tapers [2] and the hetero-core optical fibers [3], Michelson interferometer based on single mode fiber (SMF) and polyvinyl alcohol (PVA) coated photonic crystal fiber (PCF) [4], and Fabry-Perrot interferometer based on SMF and hollow core fiber with chitosan film at the fiber end [5] and the agarose gel filled PCF sensor [6]. Fiber grating incorporated structure is another promising platform for RH sensing applications because of its unique spectrum properties, such as hydrophilic material coated long-period gratings (LPGs) [7, 8] and fiber Bragg gratings (FBGs) [9,1 0], polymer fiber FBGs [11], polyvinyl alcohol (PVA) coated tilted fiber Bragg gratings (TFBGs) [12, 13]. Although these sensors can achieve relatively high sensitivity, the large spectral width [2–8, 12, 13], measurement of transmission spectrum or power [2–4, 7, 8] and especially the large cross sensitivity to other parameters such as temperature or axial stain [2–13], limit their possibility for practical applications. Recently, hybrid structures were proposed and demonstrated for simultaneous measurement of RH and temperature, for example, the modal interferometer incorporated with an FBG [14, 15] and a dielectric multilayer-based fiber-optic sensor [16].

In this letter, we present a new configuration for RH and temperature sensing based on a knob-shaped taper integrated FBG with PVA coating by using the dip coating technique. The taper here works as a multifunctional joint that not only excites the cladding modes but also recouples the reflected cladding modes back to the core mode. The PVA film is a humidity-to-refractive index transducer, modulating the reflection power of the cladding mode when

#238178 Received 16 Apr 2015; revised 31 May 2015; accepted 1 Jun 2015; published 4 Jun 2015

RH changes. The utilization of just conventional single mode fibers also has stronger mechanism, lower cost and ease of fabrication compared to the schemes cited above. Series of experiments were carried out from fabrication to RH, temperature and time response tests. The high sensitivity, fast response, long term stability and the capability for simultaneous measurements of the RH and temperature will be elaborated in the following sections.

2. Sensing principle

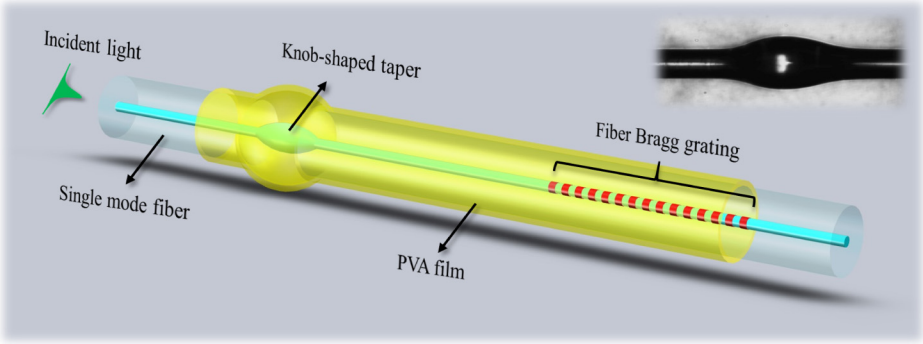

Fig. 1. The schematic diagram of our proposed sensor structure. The inset is the optical microscopy image of the fabricated knob-shaped taper.

The schematic diagram of the novel RH sensor is shown in Fig. 1. The sensing structure consists of a knob-shaped taper joint and an FBG inscribed in the downstream of a conventional SMF. It has been demonstrated the knob-shaped taper joint is a simple and promising structure for cladding mode exciting and recoupling [2]. In this case, when the light in the leading SMF reaches the taper joint, due to the waveguide expansion, the fundamental mode will spread out into the cladding and excite numerous high-order cladding modes. Assuming the knob range is ideally symmetrically expanded, only the zero order azimuthal modes are excited. Thus the launched field is decomposed into the eigenmodes LP_{0m}, as below

$$E(r,z)=\sum_{m=1}^{M} c_m \psi_m(r) e^{i\beta_m z} \tag{1}$$

where $\psi_m(r)$ is the field profile of LP_{0m}, c_m is the excitation coefficient of each eigenmode, β_m is the propagation constant of each eigenmode. The excited cladding mode then propagates along the SMF by way of total reflection between the boundary of fiber cladding and surrounding medium. Both the cladding modes and the remaining fundamental mode will be reflected by the FBG and will be coupled back into core mode by the taper joint, if they satisfy the phase matching condition for Bragg resonance

$$\lambda_m = 2n_{eff,m}\Lambda,\ \ m=1,\ 2,\ 3\cdots \tag{2}$$

where Λ is the period of FBG, m is the Bragg resonance mode order. When $m=1$, λ_1 and $n_{eff,1}$ represent the wavelength and effective RI of the fundamental mode, respectively. Otherwise λ_m and $n_{eff,m}$ represent the Bragg wavelength and effective RI of the *mth* high order cladding mode.

The final captured reflective cladding mode intensity is determined mainly by three factors: 1) the mode excitation coefficient c_m, which can be expressed by the overlap integral between $E(r,0)$ and $\psi_m(r)$. 2) the maximal reflection of the FBG $R=tanh^2(\kappa L)$, where κ is

#238178 Received 16 Apr 2015; revised 31 May 2015; accepted 1 Jun 2015; published 4 Jun 2015

the coupling coefficient which is defined by the overlap integral of Bragg mode and its identical counter-propagating mode with the UV induced index modulation, L is grating length. 3) the ambient material absorption via the evanescent field through the Beer–Lambert law. Thus the captured reflective cladding mode intensity can be expressed as

$$I_m = c_m^4 R I_{m,0} exp(-2s\alpha d) \tag{3}$$

where $I_{m,0}$ is the initial mode intensity, α is the absorption coefficient of the ambient material, d is the effective distance between the knob and the FBG. s is the relative sensitivity coefficient defined as $s = (n_{ext}/n_{eff})f$, where n_{ext} is the RI of the external material and n_{eff} is the effective RI of the Bragg mode, f is the fraction of the evanescent field intensity.

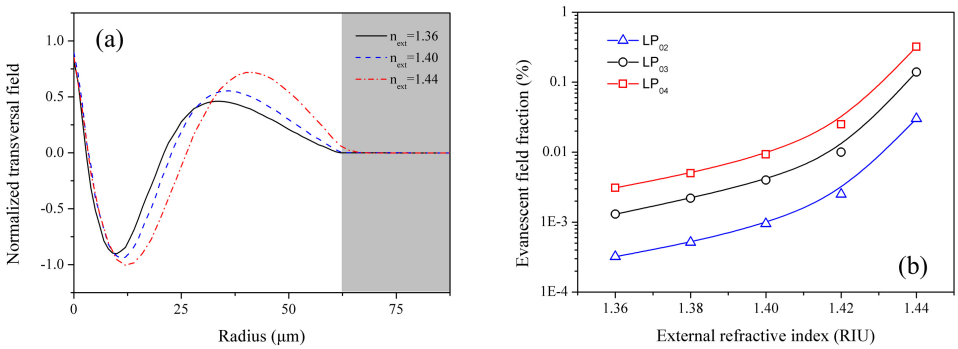

Fig. 2. (a) the transversal field evolution of LP_{03} mode under different external RIs. The gray area indicates the external surrounding. (b) Evanescent field fractions of the three cladding modes with the increase of the external RIs.

To investigate the influence of n_{ext} on the excited cladding modes, COMSOL Multiphysics finite element method software was utilized to solve for the modal distribution in the SMF. The parameters of the SMF are: core diameter of 8.3 μm, cladding diameter 125 um, core refractive index 1.4503, cladding refractive index 1.4447. Figure 2(a) gives the transversal field evolution of LP_{03} mode under different external RIs. With the increasing of n_{ext} , the $\psi_3(r)$ tends to expand to the outer cladding,which will reduce the overlap integrals of $\psi_3(r)$ with $E(r,0)$ and with the index modulation, respectively, finally causing the decrease of c_3 and R . Also the rise of n_{ext} will significantly enhance the evanescent field of the excited cladding modes (see Fig. 2(b)), which will increase the absorption loss of the cladding mode. Overall, the intensity of the captured reflective cladding mode has a negative correlation with the external RIs.

As a humidity-sensitive material, the water concentration of the PVA reaches a fast equilibrium with atmospheric moisture, which results in its RI variance from 1.49 to 1.34 when the ambient humidity increases from 20%RH to 95%RH [13]. By dip-coating it on the fiber surface of the sensing structure, the PVA film could function as a humidity-to-RI transducer. Thus, theoretically, by intensity interrogation of the reflective cladding mode, our proposed sensing structure is a potential candidate for RH measurement. On the other hand, since the FBG is instinctively sensitive to temperature fluctuations, by monitoring the wavelength of the reflected cladding mode, one can obtain the temperature information as well.

#238178 Received 16 Apr 2015; revised 31 May 2015; accepted 1 Jun 2015; published 4 Jun 2015

3. Sensor fabrication

3.1 Knob-integrated fiber Bragg grating

The proposed sensing structure has been implemented by using a commercial single mode fiber (SMF28). Before FBG fabrication, the SMF was hydrogen-loaded under 100 bar pressure for 6 days. An FBG with a length of ~5 mm was written by using the phase mask method with a 193 nm ArF excimer laser (Coherent, Bragg Star 1000). The knob-shaped taper joint was then fabricated through fusion tapering technique by manually operating a commercial fusion splicer (FITEL S177). At first, two cleaved fiber end-facets were aligned to each other in the X-Y plane. Then we move them inwards to realize physical contact and add an extra Z push of 20. After an arc discharge with duration of 30 and current of 30, the fiber locally expanded (all the parameters mentioned are relative values defined by the fusion splicer). By repeating the Z push and discharge step, while monitoring the reflection spectrum, we can obtain a knob-shaped taper as shown in the inset of Fig. 1. The distance between the taper and FBG is about 6 mm. All the parameters are determined by trials to ensure high excitement and coupling efficiency.

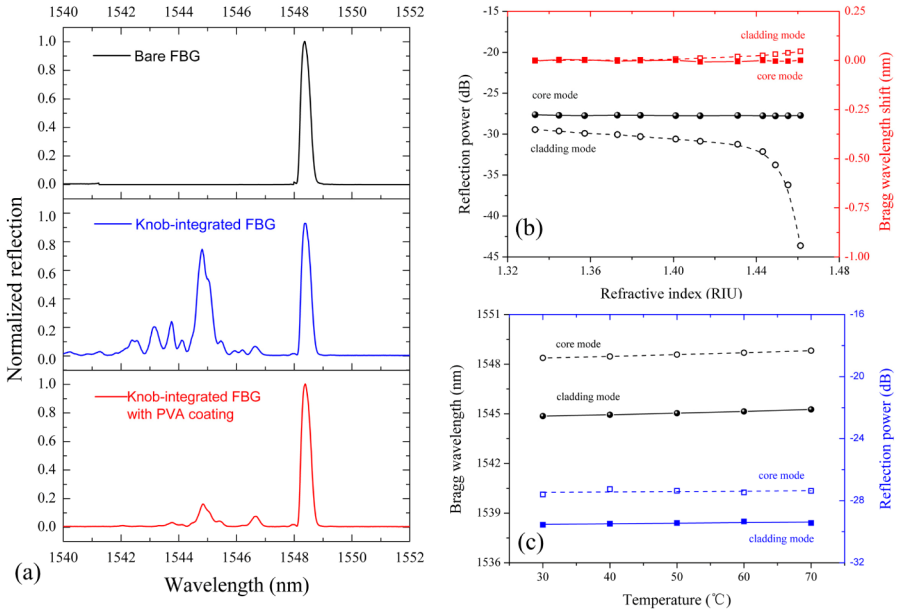

Fig. 3. (a) Spectral comparison of the bare FBG, knob-integrated FBG and PVA coated knob-integrated FBG. (b) Reflection power and Bragg wavelength changes as a function of surrounding RIs. (c) Reflection power and Bragg wavelength as a function of temperature.

Figure 3(a) shows the normalized reflection spectra of the bare FBG and the knob-integrated FBG recorded by using an optical spectrum analyzer (ANDO, AQ6317). It can be seen that there is only one reflection peak at the wavelength of ~1548.5 nm in the bare FBG reflection spectrum (see Fig. 3(a)), which corresponds to the fundamental core mode. However, when the light is launched from the taper end into the knob-integrated FBG, there exist multiple reflection peaks in the short wavelength band, corresponding to the high order cladding resonance modes (see Fig. 3(a)). The RI response of the fabricated knob-integrated FBG was tested by using a series of glycerol solutions with RI range from 1.3333 to 1.4613. As shown in the Fig. 3(b), with the RI increasing, the Bragg resonance wavelength of the cladding mode redshifts a bit with an average sensitivity of 0.5 nm/RIU (refractive index unit). However, the reflection power decays quickly and nonlinearly. One can clearly see that there are two linear regions: one is in the lower RI range of 1.3333~1.4310, with RI sensitivity of 18.6 dB/RIU. The other one is in the higher RI range of 1.4431~1.4613. In this

#238178 Received 16 Apr 2015; revised 31 May 2015; accepted 1 Jun 2015; published 4 Jun 2015

range, the RI of the measurand is higher than the RI of the fiber cladding, and the cladding modes shift to radiation modes and the reflection power plummets with an average sensitivity up to 637 dB/RIU. In this case, the investigation on intensity is a better way to interpret the RI change.

The temperature response was also measured by using a tunable oven. Figure 3(c) shows the trend of the reflection wavelength and the power as temperature increases from 30 °C to 80 °C. The cladding mode and fundamental core mode red shift almost linearly at the same rate of ~10 pm/°C. Meanwhile, the reflection power keeps constant. It is worth noting that being well confined in the fiber core, the reflection wavelength and power of the fundamental mode remain stable as in the case of RI variance, and thus makes the fundamental mode a promising temperature and light source power reference.

3.2 PVA coating

To coat the knob-integrated FBG, PVA solution was first prepared. A certain amount of PVA granules were dissolved into deionized water at 90°C with magnetic stirring for 2 hours. The fabricated sensing structure was rinsed with deionized water and dried in the air. Then the PVA was plated on the fiber surface by way of dip-coating process, by utilizing a stepper motor (SC100) with tunable pulling speed. The coated structures were dried in an oven at 80°C for 3 hours to ensure the total evaporation of the water in the protein. The thickness of the PVA film will be finally determined by the concentration of the PVA solution, which affects the viscosity of the liquid and the pulling speed.

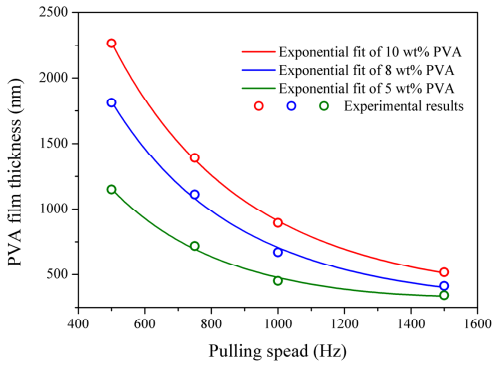

Fig. 4. Decrease trend of the thickness of PVA film as a function of pulling speed for three batches with different PVA concentrations.

The dip-coating process was carried out on the surface of the cladding of the SMF. Three batches of PVA solutions with different concentrations of 5wt%, 8wt%, and 10wt% were prepared. Four pulling speeds were set, as 500 Hz, 750 Hz, 1000 Hz and 1500 Hz (relative values defined by the stepper motor) during the dip-coating process for each batch. Finally we fabricated twelve samples with different coating thickness. To characterize the thickness and morphology of the PVA film, scanning electron microscopy (SEM) was utilized. Figure 4 shows the measured coating thickness with respect to the increment of pulling speed of each batch. One can see that the coating thickness decreases exponentially with the increment of the pulling speed and that the lower the PVA concentration is, the thinner the coating will be. The regular trend indicates that the dip-coating process is well performed in the experiment. Figure 5 shows the SEM photos of the cross section and the side view of the optical fiber with PVA coating. A uniform coating film can be confirmed from the photos. The enlarged inset shows the existence of cracks on the PVA film, which provide channels for the diffusion of the water molecules. The reflection spectrum of the knob-integrated FBG with PVA coating was recorded and given in Fig. 3(a). Due to the high RI of the PVA film (nominally $n_{PVA} \approx 1.49$), the cladding modes vanished and the reflection power decreased significantly.

#238178 Received 16 Apr 2015; revised 31 May 2015; accepted 1 Jun 2015; published 4 Jun 2015

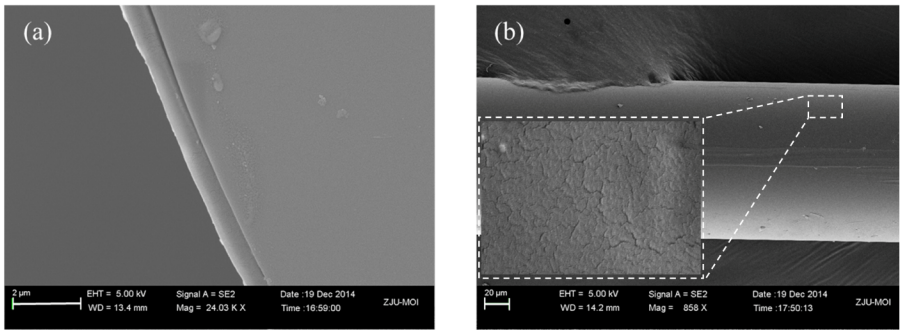

Fig. 5. The scanning electron microscopy photos of (a) the cross section and (b) the side view of the knob-integrated FBG with PVA coating.

4. Experimental results and discussion

4.1 Relative Humidity response of the sensor

Figure 6 shows the schematic diagram of the experimental setup for relative humidity response measurement. Two fabricated optic fiber sensors (with PVA coating thickness of ~892 nm, the identical FBG reflection and Bragg wavelength) were fixed on a quartz slide to avoid any bend and strain, and connected to the system by an optical switch. For relative humidity measurement, one sensing probe was inserted into a home-made humidity chamber. The humidity can be adjusted from 20%RH to 95%RH, and can be calibrated by using a commercial hygrometer (SMART SENSOR AS847) with a resolution and sampling frequency of 0.1%RH and 2.5 times/s, respectively. The reflection signal goes through a circulator and is recorded by an optical spectrum analyzer (OSA) with a resolution of 0.01 nm. Since the relative humidity is related to the temperature [16] (temperature changes causing the variance of the relative humidity), a sealed humidity chamber was made (the packaging was completed at room temperature and under ~80%RH) and placed on a hot plate, to simulate the real atmospheric conditions. For simultaneous measurement of the temperature and the relative humidity, the other sensing probe was then sealed in the other humidity chamber.

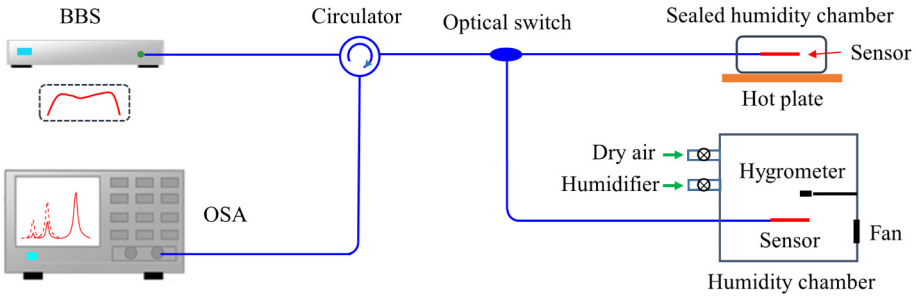

Fig. 6. Schematic diagram of the experimental setup for relative humidity and temperature measurement.

The reflection spectral evolution of the fabricated optic fiber sensor for different RH levels is given in Fig. 7(a). As the RH level rises, the hydrophilic PVA film absorbs more water, thus causing the swelling of the PVA coating and a reduction in density, which finally results in a reduction in the refractive index of the coating film. Due to the sensitivity of the cladding to the ambient RI change and to the well-confined of the core mode, one can see that as the RH rises the reflected power of the cladding modes also rises up gradually while the reflection power of the core mode remains almost constant. The reflection of the highest cladding mode was recorded and plotted as a function of relative humidity change in ascending orders, as

#238178 Received 16 Apr 2015; revised 31 May 2015; accepted 1 Jun 2015; published 4 Jun 2015

shown in Fig. 7(b). In the RH range of 30%~70%, the RI of the PVA coating decreases from 1.49 ($> n_{clad}$) to 1.43 ($< n_{clad}$), and thus the transmission condition of the cladding modes in the coating section gradually can be satisfied. The radiation loss of the cladding mode decreases and the reflection power will be enhanced progressively. When the relative humidity further increases from 70%RH to 90%RH (n_{PVA} further decreases from 1.43 to 1.34), the cladding modes are no longer the radiation modes but gradually become the guided modes, and the reflection power of the cladding modes increases by a great degree with a maximal sensitivity of up to ~1.2 dB/%RH. In the case of 95%RH, the reflection power of the cladding mode drops due to the coagulation of the water vapor on the fiber surface, which then makes it bent and adds extra strains to the sensing structure resulting in more transmission loss of the reflective cladding mode. The RH response was also carried out in the descending order of the RH to test the hysteresis. The results are shown in Fig. 7(b), which indicate that although there is a small degree of hysteresis, the detection errors remain less than 0.45%RH. The inset of Fig. 7(b) shows the reflection wavelength of the cladding mode as a function of relative humidity. One can see that the RH change has a negligible influence on the wavelength of the reflective cladding mode with an ultra-low sensitivity of 0.2 pm/10%RH, which indicates the potential for simultaneous measurement of the RH and the temperature by using intensity and wavelength demodulation, respectively. It should be noted that in the practical intensity interrogation system, it is not necessary to use an OSA to interpret the humidity information. Generally, a more effective approach is to replace the BBS with a single wavelength optical laser source and utilize a photodiode (PD) for power detection (details see 4.3 Time response of the sensor). Compared with the wavelength interrogation [2, 3, 7, 9, 11, 14–16], it not only reduces the cost of the system, but also can provide a much higher acquisition rate.

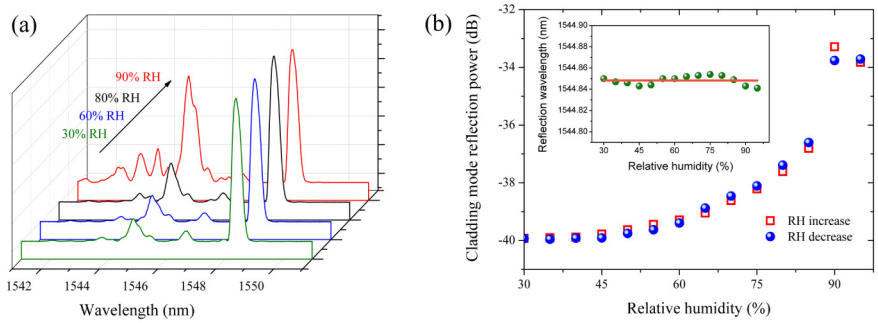

Fig. 7. (a) Reflection spectral evolution of the RH sensor under different RH levels and (b) the reflection power of the cladding mode as a function of relative humidity in both ascending and descending orders. The inset is the reflection wavelength of the cladding mode as a function of relative humidity. The orange line is the linear fit of the experimental data.

Temperature cross-sensitivity is an important parameter which needs consideration for such humidity sensors. In the preceding study, the intrinsic temperature influence on the reflection power of the cladding mode is extremely small (see Fig. 3(c)). However, the temperature dependent characteristic of the saturated water vapor pressure links the temperature change with the relative humidity. Thus the relative humidity in a sealed system varies with the change of the environmental temperature. So the humidity sensing makes sense only if we can give the temperature information at the same time. To simultaneously measure the relative humidity and temperature, the sensor was sealed in a chamber with an initial RH of 80%RH. The sealed system was then heated from 25 °C to 60 °C step by step and the reflection spectra were recorded at the interval of each temperature. As Fig. 8(a) shows, with the increment of the temperature, the reflection spectra of the cladding mode shift to a longer wavelength as expected. Meanwhile, the reflection power decreases gradually, which can be attributed to the decrease of RH caused by the temperature rise [16]. Figure 8(b)

#238178 Received 16 Apr 2015; revised 31 May 2015; accepted 1 Jun 2015; published 4 Jun 2015

shows the recorded peak power and wavelength of the cladding mode as a function of temperature. One can see a linear wavelength behavior to the temperature change with a sensitivity of ~8.2 pm/°C and a nonlinear power trend to the induced RH changes with a maximal power change of 3.01 dB. It demonstrates that by monitoring the reflection wavelength and the power of the cladding mode, our sensing structure is a promising platform for simultaneous measurement of the relative humidity and temperature of the surrounding environment.

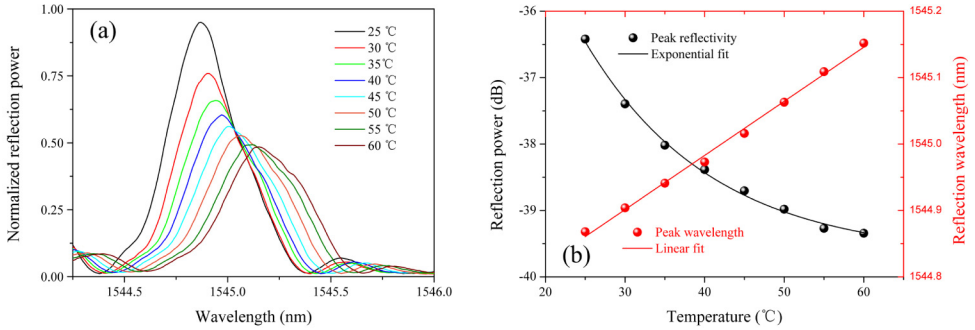

Fig. 8. (a) Reflection spectral evolution (b) Reflection power (black) and wavelength (red) response of the sealed RH sensor under different temperatures.

4.2 Time response of the sensor

Time response of the RH sensor is of great importance for practical applications. In our experiment, a tunable laser was set at 1544.800 nm, which was near the peak wavelength of the cladding resonance mode when the sensor is placed in the air at 25 °C, as shown in Fig. 7(a). The light power variation was detected by a PD and was recorded via a data acquisition card using Labview program with a sampling frequency of 100 Hz. First, the sensor reached equilibrium in the surrounding environment with a humidity of 38.7%RH. Then, it was gently moved into a chamber with humid air, where the RH was measured to be 90% with a random fluctuation of about 1%RH. One can see that the electric signal from the PD increased and reached a plateau (see Fig. 9(a)). After that, the sensor was moved out of the chamber to allow it dry in low-humid air and the signal fell down as well. A few cycles were repeated to determine the response time and the hysteresis of the sensor, as shown in Fig. 9(a). The jitters appearing in the rising and falling edges of every cycle are induced by the manual operation of the sensor. A rise time and fall time (10% base line to 90% signal maximum) were determined as 3.07 s and 3.19 s, respectively (see the enlarged cycle in Fig. 9(a)).

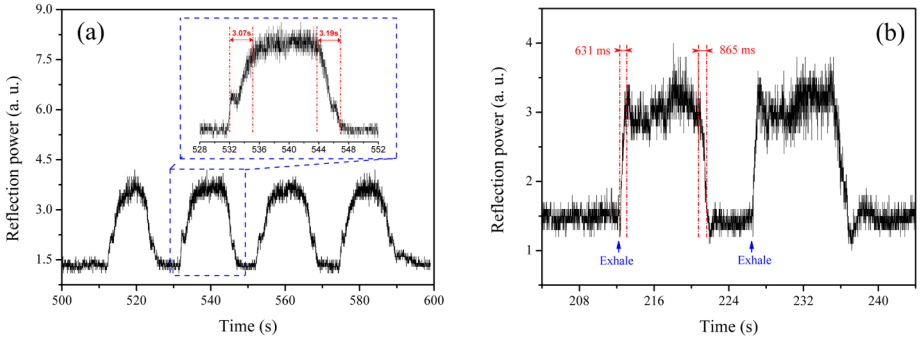

Fig. 9. Time response of the RH sensor (a) when put in and out of the chamber, (b) by exposed under human breathing.

In the former experiment, the temporal change of the humidity is mainly dominated by the manual movement of the sensor in and out of the chamber. The time response of the RH

#238178 Received 16 Apr 2015; revised 31 May 2015; accepted 1 Jun 2015; published 4 Jun 2015

sensor is believed to be much faster than the manual operating time. Thus another test to pick up human breathing was performed to verify the time response of the sensor. In this test, the humidity sensor was repeatedly exposed to a step-by-step humidity change by giving a~ 6 s long human exhalation, whose humidity was tested by a hygrometer and ensured to be above 90%RH. The ambient humidity during the test was ~38.7%RH and the temperature was ~25 °C. Figure 9(b) shows the temporal profile of the electric signal when the human exhalation was given. The rising time and the falling time can be estimated as ~631 ms and ~865 ms, respectively, which is much faster than the response times in the former test. Meanwhile, it is shown that the two profiles of the test cycles look similar with only a tiny difference induced by each exhalation manner, which indicates an excellent repeatability and potential to pick up the humidity change as fast as 630 ms.

4.3 Stability and repeatability tests

For further investigating its practical sensing performance, the stability and repeatability tests of our proposed humidity sensor were carried out as well. In the stability test, the fabricated humidity sensor was placed in the homemade chamber under constant RHs of 70% and 90%, respectively. Each measurement lasted more than 2 hours and the cladding mode reflection power was recorded every 10 mins. Figure 10(a) presents the results of the stability test and we can see that a maximal fluctuation of less than 0.13 dB over the period of 140 minutes, which may be caused by the power fluctuation of the light source. To further depress this error, one can utilize the fundamental core mode as power reference. In order to test the repeatability, six batches of measurements were performed. Three of them were carried out right after the fabrication of humidity sensor and the other three measurements were completed after two months of the initial experiments. The similar response trends with error bars are shown in Fig. 10(b). Considering the errors in the measurements, the sensing accuracy varies from ±2%*RH* to ±4.5%*RH* in the low RH range of 30-70%RH, and remains about ±1%*RH* in the high RH range of 70~90%RH, which confirms a good repeatability and an excellent long term stability.

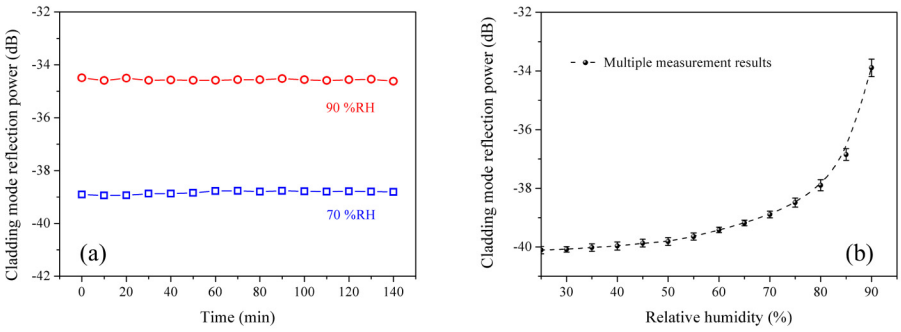

Fig. 10. (a) Stability test of the proposed humidity sensor under constant RHs of 70 and 90% RH, respectively. (b) Repeatability test of the humidity response. Error bars are calculated from six experimental measurements.

5. Conclusion

We have presented a novel RH and temperature sensor that we have newly designed based on a knob-integrated FBG. The polyvinyl alcohol sensing film, which acted as a humidity-to-refractive index transducer, was made by dip-coating technique and its morphology was characterized by using SEM. The RH and temperature response of the proposed structure has been experimentally tested and examined. The results show that a 6.58 dB increase of the reflection cladding mode power could be obtained in the RH range of 30-95%RH and the temperature information could be interpreted by monitoring the reflection wavelength of the cladding mode. The time response of the humidity sensor was also measured by two methods.

#238178 Received 16 Apr 2015; revised 31 May 2015; accepted 1 Jun 2015; published 4 Jun 2015

Especially, the human breathing test confirms that the RH sensor can pick up the humidity change as fast as 630 ms. The capability of simultaneous measurement of the RH and temperature, the fast response, the reusability and the simple fabrication process make our proposed structure a highly promising sensor for real-time RH monitoring.

Acknowledgment

This work was supported by the Program of Zhejiang Leading Team of Science and Technology Innovation (2010R50007) and the National Natural Science Foundation of China (91233208) and the National High Technology Research and Development Program of China (2012AA012201).

#238178 Received 16 Apr 2015; revised 31 May 2015; accepted 1 Jun 2015; published 4 Jun 2015